Supplementary Information

Graphitic Domain Layered Titania Nanotube Arrays for Separation and Shuttling of Solar-Driven Electrons

Dong Ki Lee [a], Kyu Sung Han [a], Weon Ho Shin [a], Jung Woo Lee [a], Jung Hoon Choi [a], Kyung Min Choi [a], Yeob Lee [a], Hyoung-il Kim[d], Wonyoung Choi[d] and Jeung Ku Kang *[a,b,c]

[a] Department of Materials Science & Engineering, [b]Graduated School of EEWS (WCU), and [c] NanoCentury KAIST Institute, Korea Advanced Institute of Science and Technology (KAIST), 291 Daehak-ro, Yuseong-gu, Daejon 305-701, Republic of Korea,

*E-mail: jeungku@kaist.ac.kr

[d] School of Environmental Science and Engineering, Pohang University of Science and Technology (POSTECH), Pohang, 790-784, Korea

Contents

Experimental

Fabrication of anodized TiO_2 NTs: Ti foil (99.7%, ALDRICH) was ultrasonically cleaned with acetone, ethanol, and water for 1 hour, respectively, and was dried in nitrogen flow. Anodization was performed in a two-electrode configuration with Ti foil (1×1 cm^2) as the cathode and Ni foil (99.9%, ALDRICH) as the anode with mild stirring at room temperature. The electrolyte was prepared using an ethylene glycol solution with 0.25 wt% NH_4F (99.99%, ALDRICH) and 1 vol.% of water. The anodic growth of the TiO_2 NTs was carried out for 4 hour at 60V with direct current (DC) power supply (AGILENT E3612A). The obtained NTs were annealed at 650°C for 2 hours to obtain the anatase phase. Heating and cooling rates were 1°Cmin^{-1}

Formation of graphitic domains: Prepared bare TiO_2 NT arrays were first immersed in a 70 mL aqueous solution of certain concentration glucose (99.5%, SIGMA) for 5 hours. Subsequently, the mixture containing TiO_2 NT arrays was transferred to a 100 mL Teflon-lined stainless steel autoclave and heated at 180°C for 5 hours for polymerization. After rinsing with ethanol and water several times, samples were dried in a 70°C vacuum oven for at least one day. Then, samples were pyrolyzed at 650°C under argon (99.999%) flow at 300 torr for 3 hours. Heating and cooling rates were 2°C/min.

Characterizations: The microscopic features of the samples were observed by JEOL JSM-7401F and a HITACHI S-4800 SEM, and JEOL JEM-ARM200F TEM and STEM. The EELS profiles are collected with GATAN Quantum SE. The energy dispersive spectrometer (EDS) images were observed by using a BRUKER QUANTAX EDS for TEM. The crystal structures were measured by thin film XRD patterns which were carried out using a RIGAKU D/MAX-2500 with monochromatized Cu Kα radiation, and scanning at a 2°min^{-1} with an angular resolution of 0.01°. Raman spectra were acquired with a LabRAM HR UV/Vis/NIR (Horiba Jobin Yvon) high resolution dispersive Raman microscope using an argon ion laser (514.5 nm). XPS analysis was carried out a THERMO SCIENTIFIC Sigma Probe. The monochromatized Al Kα was used as the photon source.

Optical and PEC Measurements: The diffused reflectance spectra were determined by a VARIAN Cary-300 UV-vis spectrophotometer with DRA-CA-30I. The bare Ti foil was used for the baseline. The florescence spectra were determined by LabRAM HR UV/Vis/NIR photoluminescence (Horiba Jobin Yvon) with 325 nm He-Cd CW laser source. The florescence decay spectra with the TCSPC system was measured using Edinburgh Instruments FL920. The emission peak at 509 nm that was excited by 375 nm laser source (1 MHz) was collected to by the TCSPC detector at 18°C. The PEC measurements were carried out in a conventional three-electrode system connected to a potentiostat (Gamry, Reference 600). A platinum wire and an Ag/AgCl electrode were used as counter and reference electrodes, respectively, which were immersed in aqueous electrolyte of 0.1M $NaClO_4$ with 25 vol.% methanol. The electrolyte solution was continuously purged with nitrogen during measurement and the NEWPORT 300 W Xenon lamp with air mass (AM) 1.5G (100 $mWcm^{-2}$) light filter was used for light source. The scan rate for the voltammogram was 10 mVs^{-1}. The values from EIS were obtained at open-circuit potential (OCP) in the frequency range of $10^6 \sim 10^{-2}$ Hz. The optical system for the photocatalytic reactions was composed of a NEWPORT 300 W Xenon arc lamp and an IR filter ($\lambda > 700$ nm) with water cooling system. The average light intensity was 300 $mWcm^{-2}$. The quartz reactor was filled with 62 ml water solution of 25 vol.% methanol and purged with helium (99.999%) for about 2 hour. The evolution of hydrogen was carried out without Pt and reference electrode, and monitored by using SHIMAZU GC-2014A gas chromatograph of closed circulation system with quartz reactor.

Sample	**TiO_2 annealing temperature (°C)**	**Glucose concentration (mmol)**	**Pyrolysis temperature (°C)**
TiO_2 NT	650		
GDN-1	650	1	650
GDN-5	650	50	650
GDN-10	650	100	650
TiO_2 NT-7	750		
GDN-17	650	1	750
GDN-57	650	50	750
GDN-107	650	100	750

Table S1. The experimental conditions of various samples.

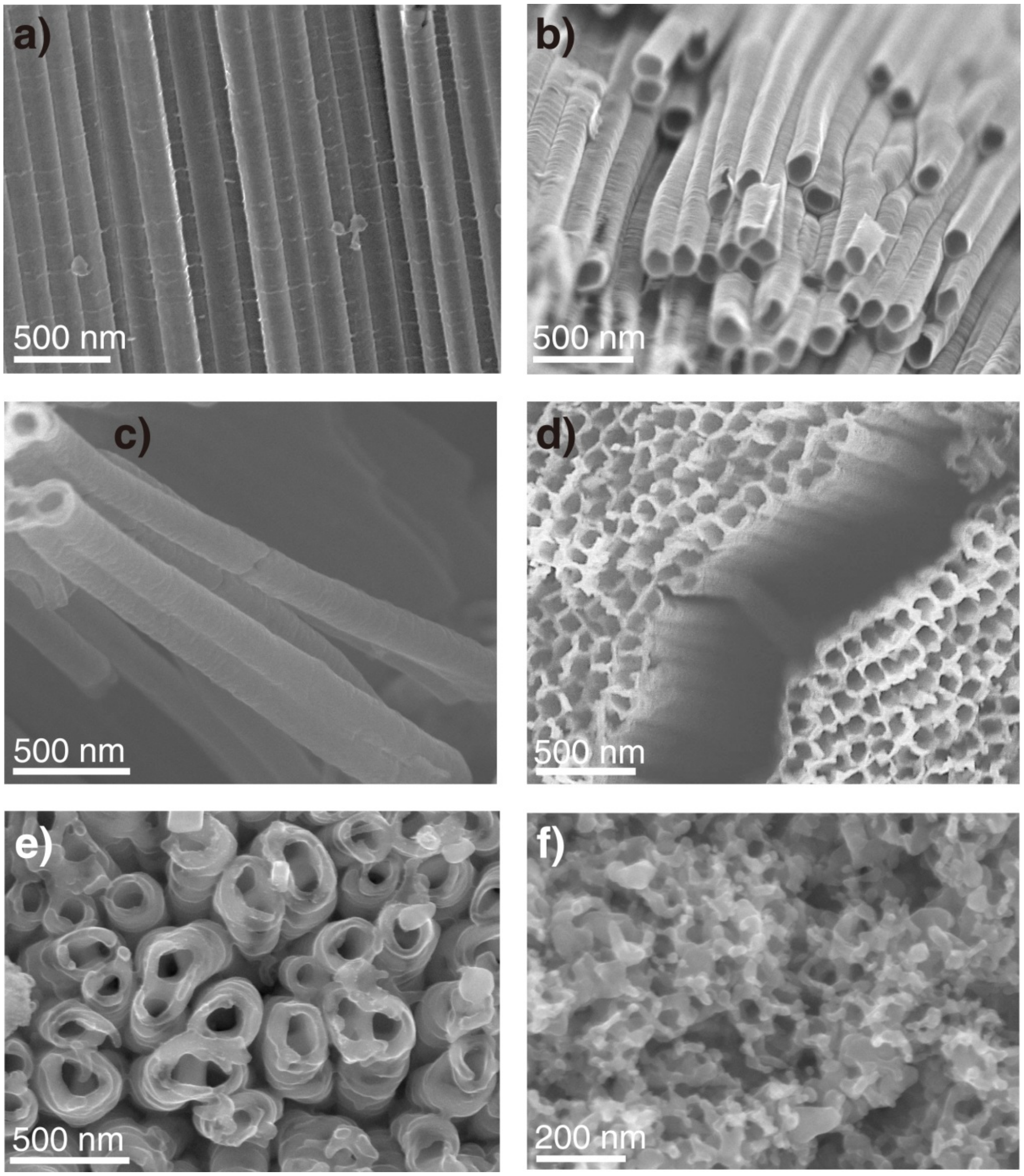

Figure S1. FE-SEM images of bare TiO_2 NTs **a**) before and **b**) after annealing at 650°C. The smooth surface is changed to uneven. **c**) FE-SEM image after hydrothermal treatment. Polymerized glucose covers whole surface of TiO_2 NTs. Top views of **d**) GDN-5, **e)** GDN-10 and **f)** GDN-57 samples, respectively. The original ordered and aligned 1-D morphology of TiO_2 NTs of GDN-5 is preserved well after the creation of graphitic carbon layer. However, excess of carbon (GDN-10) and high pyrolysis temperature (GDN-57) introduce collapse of original morphology of TiO_2 NTs.

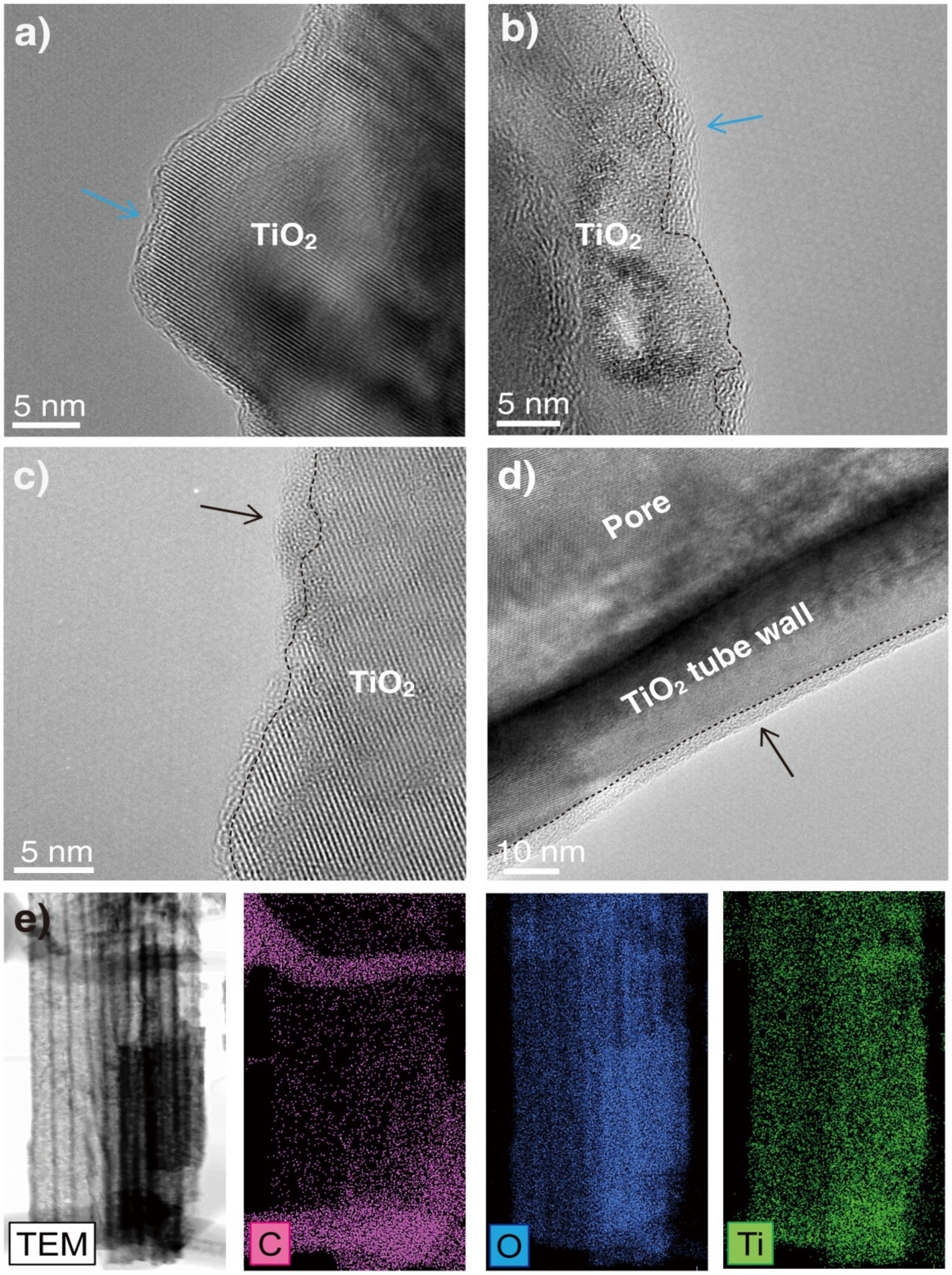

Figure S2. HR-TEM images for **a**) irregular, **b**) thick and fragmented shape, **c**) the amorphous states of carbons and **d**) naturally contaminated amorphous carbons on the surface of bare TiO_2 NT. **e)** Energy dispersive spectroscopy (EDS) map images of GDN-5. All elements are uniformly located throughout the surface of TiO_2 NTs.

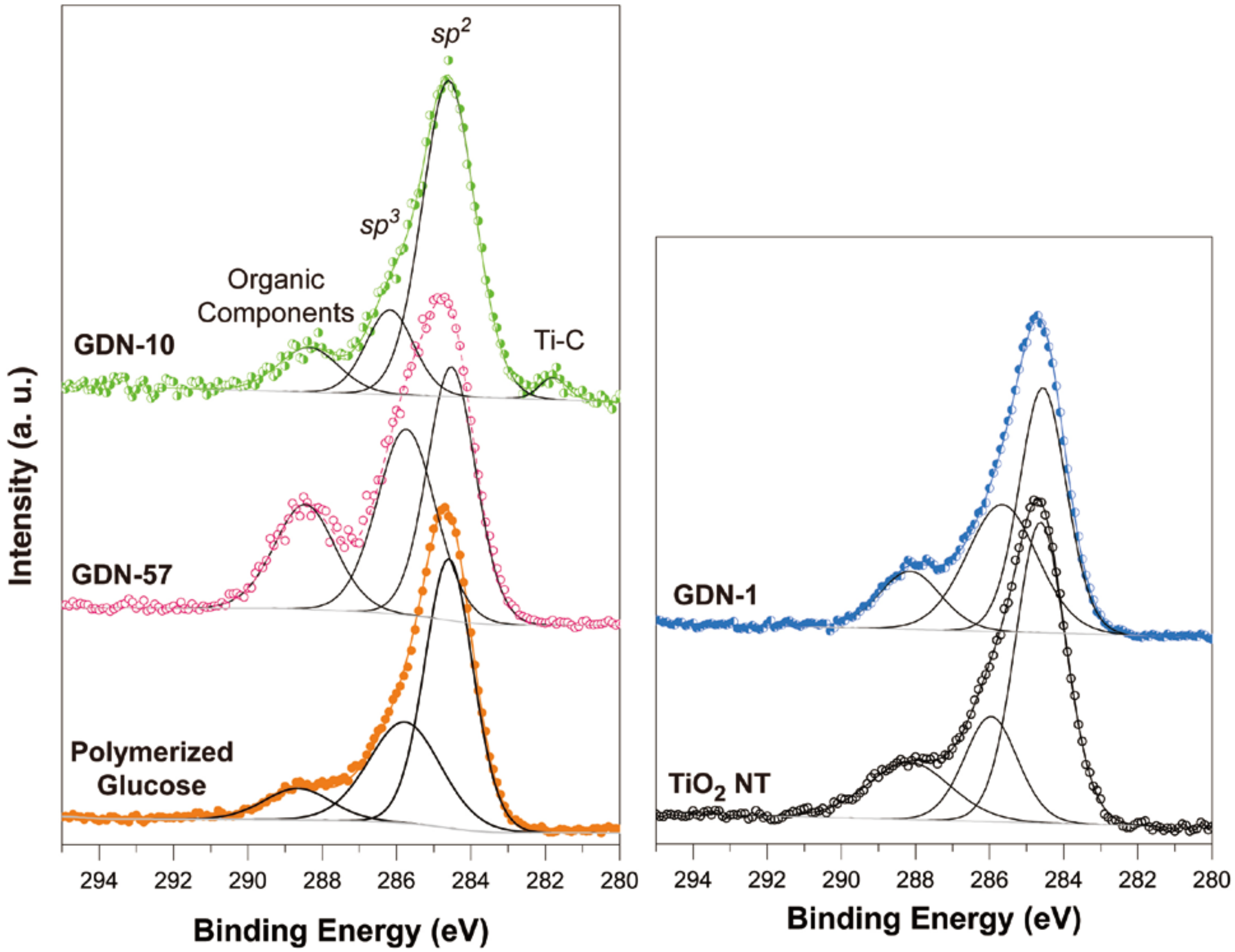

Figure S3. XPS C 1s spectra of other samples. The GDN-10 shows Ti-C bond peak. The strong *sp*^{3} and organic component peak indicate that the carbon layers of GDN-57 supposed to be amorphous state. The GDN-1 has similar peak shape with the bare TiO_2 NTs.

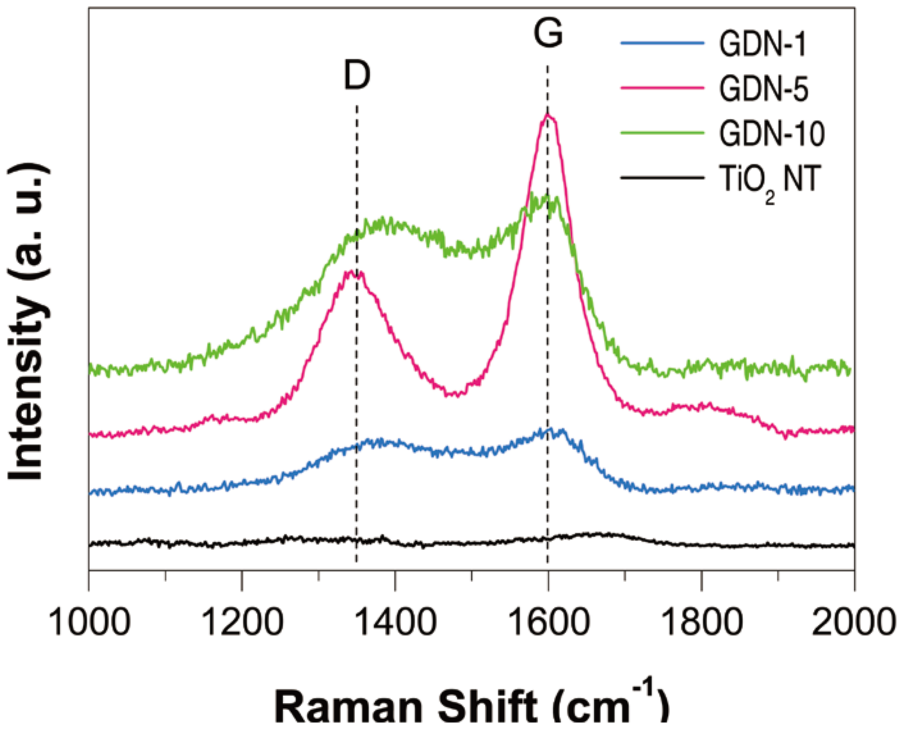

Figure S4. Raman spectra of GDN-1 and GDN-10 (GDN-5 and TiO_2 NT result are same with Figure 2a). The I_D/I_G value of GDN-1 and GDN-10 are 0.86 and 0.88, respectively. The lowest I_D/I_G value (0.56) and sharp G-band of the GDN-5 indicates that the state of carbons in GDN-5 is more graphitic than others.

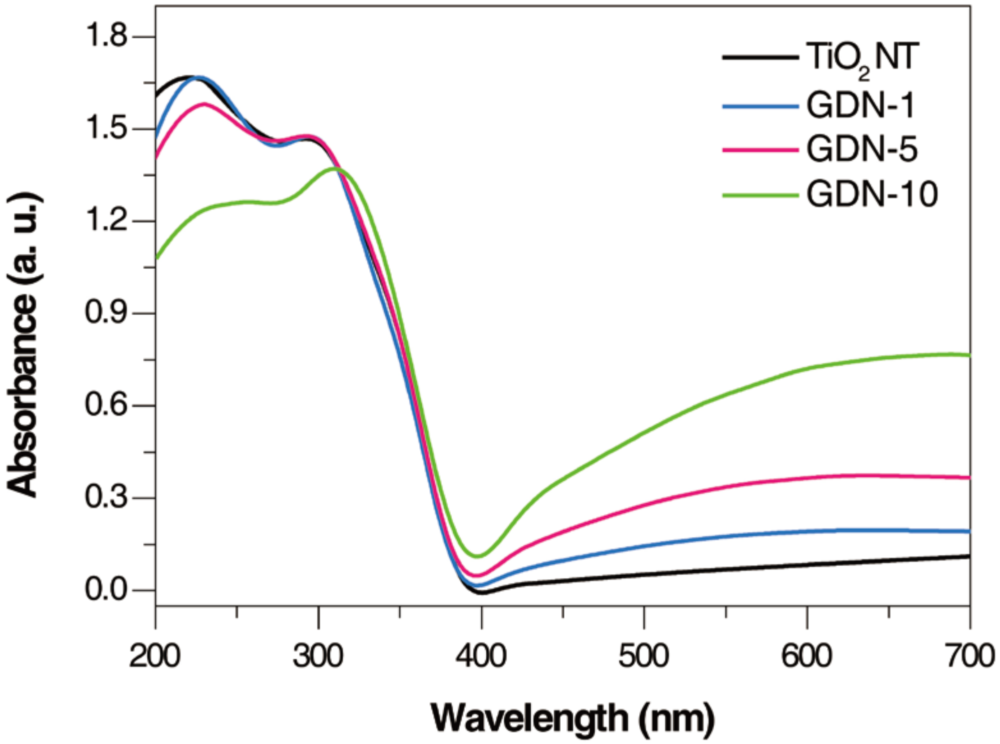

Figure S5. Diffused ultraviolet-visible (UV-Vis.) absorbance spectra. The absorbance curves of GDN-1 and GDN-5 within the UV range (200–400 nm) were similar to those of bare TiO_2 NTs. However, GDN-10 has a very different absorbance slope and intensity because of its deconstructed anatase phase (band gap: 3.2 eV) and its newly oriented rutile phase (band gap: 3.0 eV). Although GDs absorb visible light with an increase in the glucose concentration, we confirmed experimentally that they show no photocatalytic activity in the visible light range (400~700 nm). Therefore, this absorbance in the visible light range is thought to come from the molecular vibrations of various organic components that are created during the formation of GD.

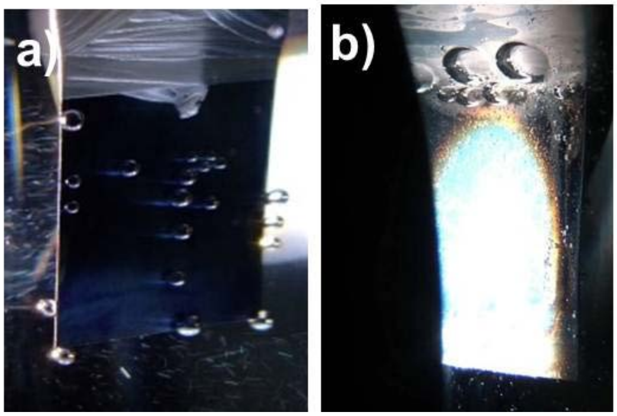

Figure S6. a) Back and **b)** front side picture of GDN-5 during hydrogen evolution in water solution of 25 vol.% methanol. Hydrogen evolution is mainly occur on GD combined TiO_2 NTs at front side, and also small amount hydrogen evolved at back side by transported electrons to titanium metal.

Sample	**Decay time (ns)**			**Relative amplitude (%)**			**Average lifetime (ns)**	χ^2
	τ_1	τ_2	τ_3	f_1	f_2	f_3		
TiO_2 NT	0.14	0.86	5.77	25.25	61.38	10.37	3.36	1.325
TiO_2 NT:Pt	0.11	0.43	3.18	55.20	42.82	1.98	0.91	1.018
GDN-5	0.12	0.57	4.21	41.82	53.14	5.04	1.89	1.175

Table S2. Tri-exponential function fitted fluorescence decay data. The average lifetime was calculated using equation (1).[32]

$$< \tau >= \frac{f_1\tau_1^2 + f_2\tau_2^2 + f_3\tau_3^2}{f_1\tau_1 + f_1\tau_2 + f_1\tau_3} \qquad (1)$$

Sample	**R_s (Ω)**	**R_{ct} (Ω)**	**CPE ($mF\cdot s^{\alpha-1}$)**	**α**
TiO_2 NT	65.18	3026	1.95×10^{-3}	0.9039
GDN-5	38.68	2419	1.56×10^{-3}	0.9015

Table S3. The fitted EIS parameters from the equivalent electrical circuit model containing constant phase element on open-circuit potential.